Title

High-Resolution CT Imaging of the Temporal Bone: A Cadaveric Specimen Study.

Journal

Journal of neurological surgery. Part B, Skull base, 83(5)

ISSN

2193-6331

Authors

Pham, Nancy
Raslan, Osama
Strong, Edward B
et al.

Publication Date

2022-10-01

DOI

10.1055/s-0041-1741006

Peer reviewed

High-Resolution CT Imaging of the Temporal Bone: A Cadaveric Specimen Study

Nancy Pham[1] Osama Raslan[2] Edward B. Strong[3] John Boone[2] Arthur Dublin[2] Shuai Chen[4] Lotfi Hacein-Bey[2]

[1] Department of Radiology, University of California, Los Angeles, California, United States
[2] Department of Radiology, University of California, Davis, Sacramento, California, United States
[3] Department of Otolaryngology, University of California, Davis, Sacramento, California, United States
[4] Division of Biostatistics, Department of Public Health Sciences, University of California, Davis, California, United States

Address for correspondence Nancy Pham, MD, Department of Radiology, University of California, 757 Westwood Plaza, Suite 1621D, Los Angeles, CA 90095-7532, United States (e-mail: pham.nancy@gmail.com).

J Neurol Surg B Skull Base 2022;83:470–475.

Abstract

Objective Super-high and ultra-high spatial resolution computed tomography (CT) imaging can be advantageous for detecting temporal bone pathology and guiding treatment strategies.

Methods Six temporal bone cadaveric specimens were used to evaluate the temporal bone microanatomic structures utilizing the following CT reconstruction modes: normal resolution (NR, 0.5-mm slice thickness, 512^2 matrix), high resolution (HR, 0.5-mm slice thickness, $1{,}024^2$ matrix), super-high resolution (SHR, 0.25-mm slice thickness, $1{,}024^2$ matrix), and ultra-high resolution (UHR, 0.25-mm slice thickness, $2{,}048^2$ matrix). Noise and signal-to-noise ratio (SNR) for bone and air were measured at each reconstruction mode. Two observers assessed visualization of seven small anatomic structures using a 4-point scale at each reconstruction mode.

Results Noise was significantly higher and SNR significantly lower with increases in spatial resolution (NR, HR, and SHR). There was no statistical difference between SHR and UHR imaging with regard to noise and SNR. There was significantly improved visibility of all temporal bone osseous structures of interest with SHR and UHR imaging relative to NR imaging ($p < 0.001$) and most of the temporal bone osseous structures relative to HR imaging. There was no statistical difference in the subjective image quality between SHR and UHR imaging of the temporal bone ($p \geq 0.085$).

Conclusion Super-high-resolution and ultra-high-resolution CT imaging results in significant improvement in image quality compared with normal-resolution and high-resolution CT imaging of the temporal bone. This preliminary study also demonstrates equivalency between super-high and ultra-high spatial resolution temporal bone CT imaging protocols for clinical use.

Keywords
- CT
- temporal bone
- ultra-high resolution
- super-high resolution

received
January 19, 2021
accepted after revision
November 12, 2021
published online
January 31, 2022

Georg Thieme Verlag KG,
Rüdigerstraße 14,
70469 Stuttgart, Germany

DOI https://doi.org/10.1055/s-0041-1741006.
ISSN 2193-6331.

Table 1 CT technical parameters on the ultra-high-resolution CT system utilizing the NR, HR, SHR, and UHR modes

Scanner parameter	Different reconstruction modes on the ultra-high-resolution CT system			
	Normal resolution (NR)	High resolution (HR)	Super-high resolution (SHR)	Ultra-high resolution (UHR)
Matrix size	512 × 512	1,024 × 1,024	1,024 × 1,024	2,048 × 2,048
Minimum slice thickness	0.5 mm	0.5 mm	0.25 mm	0.25 mm
Focal spot	0.4 × 0.5 mm			
Detector	0.25 mm × 160 rows			

Introduction

The temporal bone presents specific imaging challenges because of the complex anatomic interconnectivity, very small size, and 3D orientation of the osseous structures intrinsic to the auditory apparatus. Imaging complexity is further compounded by the confined space in which these structures are housed in. The advent of multidetector row computed tomography (CT) has improved the visualization of temporal bone anatomical landmarks[1,2] and the diagnosis of temporal bone pathology including tumors, inflammation, hearing loss, trauma, and cerebrospinal fluid leaks.[3–10] However, the clinical impact of greater anatomic detail provided by super-high and ultra-high spatial resolution CT imaging can be even more significant for improving the diagnosis, treatment, and surgical planning of temporal bone disease.[11,12] Minute temporal bone structures including the ossicular chain, the crus of the stapes, the greater superficial petrosal nerve, and the anterior malleolar ligament are better visualized on ultra-high spatial resolution CT compared with conventional CT.[13]

This study aims at assessing comparative CT image quality of the temporal bone utilizing the following reconstruction modes on an ultra-high-resolution CT imaging system (Aquilion Precision, Canon Medical Systems, Japan): normal resolution (NR), high resolution (HR), super-high resolution (SHR), and ultra-high resolution (UHR). More specifically, we will compare the imaging quality between SHR and UHR CT to determine the most optimal and clinical feasible CT protocol for temporal bone imaging in a busy clinical setting.

Materials and Methods

Ex Vivo Specimens

Three cadaveric head specimens were obtained from the Body Donation Program. Six total temporal bone specimens (accounting for bilaterality) were imaged utilizing the following reconstruction modes: NR, HR, SHR, and UHR. The use of cadaveric specimens was essential in eliminating radiation dose from being a limiting factor in this comparative analysis.

CT Protocol

CT images were obtained on the Aquilion Precision with 0.25- to 0.50-mm slice thickness, focus size 0.4 × 0.5 mm, pitch 0.6, display field of view of 100 mm, 250 mAs, collimation 20 mm, rotation time 500 ms, and helical mode at 120 kV. Images were reconstructed with filtered back projection (manufacturer's reconstruction kernel of FC35) to maintain the highest degree of osseous detail. Detailed CT parameters for the different reconstruction modes were: NR mode (0.5-mm slice thickness, 5122 matrix), HR mode (0.5-mm slice thickness, 1,0242 matrix), SHR mode (0.25-mm slice thickness, $1{,}024^2$ matrix), and UHR mode (0.25 mm slice thickness, $2{,}048^2$ matrix) (►**Table 1**).

Quantitative Image Analysis

Image noise was measured in the cadaveric images as the standard deviation (SD) of CT numbers (HU) in a circular region of interest (ROI) drawn in a uniform area for each dataset in the petrous temporal bone and air. The size and the location of the ROIs were matched among the four image sets (UHR, SHR, HR, and NR). The mean and SD of image noise for each image set were calculated. The signal-to-noise ratio (SNR) in the petrous temporal bone and the SNR in air was defined as the CT number (HU) divided by the image noise (SD) in the ROI. The mean and SD of SNR for each image set were calculated.

Qualitative Analysis

Qualitative assessment was performed on three left and three right cadaveric temporal bones. Two board-certified radiologists (2.5 and 3 years of experience) blinded to the CT parameters analyzed the images independently. The image datasets were displayed using temporal bone windows (window width: 5,100; windows level, 850).

Seven small anatomic structures were selected for the purpose of this study by a neuroradiologist. Five elements were chosen based on the perceived difficulty of visualization on normal-resolution CT based on our institutional experience (anterior crus stapes, posterior crus stapes, incudomalleolar articulation, incudostapedial articulation, and spiral osseous lamina of the cochlea). Two larger structures (cochlear and vestibular aqueducts) were selected since they are typically seen with normal-resolution CT. All images were visualized on a separate research PACS (Phillips Healthcare, Andover, MA).

Image quality was scored using a semiquantitative 4-point scale: 4, excellent delineation of structure; 3, good delineation of structure; 2, fair delineation of structure; and 1, poor delineation of structure.

Radiation Dosimetry

The CT dose index (CTDIvol) was 18.5 mGy for the UHR and SHR modes. The CTDIvol was 18.3 mGy for the HR and NR modes.

Statistical Analysis

Qualitative Analysis

Kappa (κ) statistics were used as a measure of interobserver agreement between two readers. A κ statistic in the range of 0.81 to 1 was interpreted as excellent agreement, 0.61 to 0.80 as substantial, 0.41 to 0.60 as moderate, 0.21 to 0.40 as fair, and 0 to 0.20 as poor. We calculated the point estimate of weighted κ for ordinal data using quadratic weighting, which is unbiased accounting for the correlation within the cluster (3).

Ordinal logistic mixed-effects models were used to compare the 4-point scale resulting from the four scanning methods, with random intercepts for participant, rater, and scan location within each participant to account for correlation in the clustered data. The fixed effects include scan method, structure, and their interaction. A two-sided $p < 0.0083$ (=0.05/6) for multiple comparisons using the Bonferroni correction was considered statistically significant.

Data were analyzed using R 3.6.1 (R Foundation for Statistical Computing, Vienna, Austria) for κ statistic, and GLIMMIX procedure with ESTIMATE in SAS v9.4 (SAS Institute, Cary, NC) for ordinal logistic mixed-effects models.

Quantitative Analysis

Differences in image noise and SNR between the NR, HR, SHR, and UHR groups were assessed with Student's *t*-test. A $p < 0.05$ was considered significant.

Results

Image Quality

Qualitative Results

Qualitative image scores are shown in ►**Table 2**. The interobserver agreement between the two readers was substantial (κ = 0.76). There was no statistical difference between the UHR and SHR modes for visualizing the osseous structures of interest. Compared with the NR mode, there was improved visualization of the temporal bone osseous structures with the HR, SHR, and UHR modes. There was improved visualization of four structures (posterior crus of the stapes, incudostapedial articulation, spiral osseous lamina of the cochlea, and vestibular aqueduct) with the SHR mode compared with the HR mode. There was improved visualization of all osseous structures except for the cochlear aqueduct with the UHR mode compared with the HR mode.

Quantitative Results

Quantitative evaluation of image quality is shown in ►**Table 3**. There was no significant statistical difference in image noise and SNR between the UHR and SHR images. However, there was progressively increased image noise and

Table 2 Qualitative analysis scores of UHR, SHR, HR, and NR CT images

	Reconstruction modes				*p*-Values					
Structures	UHR	SHR	HR	NR	UHR vs. SHR	UHR vs. HR	UHR vs. NR	SHR vs. HR	SHR vs. NR	HR vs. NR
Anterior crus stapes	3.33 (0.78)	3 (0.60)	2.50 (0.67)	1.17 (0.39)	0.085[a]	<0.001	<0.001	0.022[a]	<0.001	<0.001
Posterior crus stapes	3.33 (0.78)	3.08 (0.67)	2.50 (0.67)	1.17 (0.39)	0.191[a]	<0.001	<0.001	0.007	<0.001	<0.001
Incudomalleolar articulation	3.92 (0.29)	3.67 (0.49)	3.17 (0.58)	1.67 (0.65)	0.131[a]	0.001	<0.001	0.017[a]	<0.001	<0.001
Incudostapedial articulation	3.67 (0.49)	3.50 (0.52)	2.92 (0.29)	1.33 (0.49)	0.368[a]	0.001	<0.001	0.006	<0.001	<0.001
Spiral osseous lamina of the cochlea	3.75 (0.45)	3.83 (0.39)	3.08 (0.51)	1.08 (0.29)	0.599[a]	0.002	<0.001	0.001	<0.001	<0.001
Vestibular aqueduct	3.75 (0.45)	3.92 (0.29)	3.08 (0.29)	1.92 (0.29)	0.273[a]	0.002	<0.001	0.001	<0.001	<0.001
Cochlear aqueduct	3.58 (0.51)	3.67 (0.49)	3.33 (0.78)	1.92 (0.29)	0.653[a]	0.287[a]	<0.001	0.14[a]	<0.001	<0.001

Abbreviations: HR, high resolution; NR, normal resolution; SHR, super-high resolution; UHR, ultra-high resolution.
Note: Image quality was scored using a semiquantitative 4-point scale: 4, excellent delineation of structure; 3, good delineation of structure; 2, fair delineation of structure; and 1, poor delineation of structure [mean (SD)]. *p*-Values were obtained from tests based on ordinal logistic mixed effects models. The Bonferroni correction was used to adjust for multiple comparisons with a $p < 0.0083$ (=0.05/6) considered as significant.
[a]Not significant.

Table 3 Comparison of image noise and SNR between the different CT reconstruction modes

	Reconstruction modes				*p*-Values				
	UHR	SHR	HR	NR	UHR vs. SHR	UHR vs. HR	UHR vs. NR	SHR vs. HR	SHR vs. NR	HR vs. NR
Image noise										
Bone	203.59 (27.10)	209.95 (10.30)	174.32 (17.12)	132.56 (20.87)	0.58[a]	0.01	0.01	<0.01	0.03	0.01
Air	144.27 (21.99)	153.13 (13.20)	119.26 (11.29)	84.36 (22.47)	0.23[a]	0.03	<0.01	0.01	<0.01	0.01
SNR										
Bone	9.23 (1.16)	8.78 (0.56)	10.59 (1.13)	14.59 (2.30)	0.35[a]	0.01	0.01	<0.01	<0.01	0.02
Air	6.56 (0.98)	6.03 (0.53)	7.80 (0.79)	12.29 (4.80)	0.12[a]	0.02	0.02	0.01	0.02	0.06[a]

Abbreviations: HR, high resolution; NR, normal resolution; SHR, super-high resolution; SNR, signal-to-noise ratio; UHR, ultra-high resolution.

Note: The image noise and SNR of bone and air are listed [mean (SD)] without significant statistical difference between the ultra-high-resolution and super-high-resolution CT images. There is progressively increased image noise and decreased SNR with the normal-resolution, high-resolution, and super/ultra-resolution CT images, respectively. A $p < 0.05$ was considered significant. Image noise was measured as the standard deviation (SD) of CT numbers (HU) in a circular ROI drawn in a uniform area for each dataset in the petrous temporal bone and air. The size and the location of the ROIs were matched among the four image sets (UHR, SHR, HR, and NR). The mean and SD of image noise for each image set were calculated. The signal-to-noise ratio (SNR) in the petrous temporal bone and the SNR in air was defined as the CT number (HU) divided by the image noise (SD) in the ROI. The mean and SD of SNR for each image set were calculated.

[a]Not significant.

decreased SNR with the NR, HR, and SHR/UHR images, respectively.

Discussion

Technical Innovation

While many factors will impact the final spatial resolution of a CT system, detector size is one of the critical factors limiting the ability to resolve submillimeter anatomic structures. Several methods of reducing the detector element size in CT have been investigated. First, placement of an attenuating comb (grid) filter on top of the detector can reduce the detector aperture size.[14–16] However, the removable comb can block up to three-quarters of incident photons, reducing dose efficiency and limiting its clinical utility.[17,18] Second, flat panel prototype CT scanners have been studied, but are limited by contrast-to-noise ratio, scan field of view, and temporal resolution, limiting their commercialization.[19–22] Finally, recent advances in photon-counting detectors (PCDs) have made whole-body photon-counting CT possible, resulting in a variety of clinical applications, including temporal bone imaging. Ultra-high-resolution PCD-CT acquisitions can lead to superior temporal bone imaging quality, and have been shown to delineate temporal bone anatomic structures better than comb-based ultra-high-resolution modes on conventional CT scanners.[17]

The current ultra-high-resolution CT system is unique because of the following innovations: thinner detector elements (0.25 mm at isocenter), increased number of detector rows, smaller X-ray tube focus size, decreased slice thickness, and larger reconstruction matrices (►**Table 1**). By optimizing the relationships between these CT parameters, one of the most advantageous features of an ultra-high-resolution imaging CT system is the improved spatial resolution of up to 150 µm.[23,24] To our knowledge, this is the first study to directly compare the difference in image quality of the temporal bone using the NR, HR, SHR, and UHR reconstruction modes (►**Fig. 1** and ►**Fig. 2**) on this CT system. Despite the relative increase in image noise and decrease in SNR, temporal bone SHR and UHR CT imaging results in significant improvement in image quality compared with NR and HR imaging (►**Fig. 1** and ►**Fig. 2**). A prior study has shown excellent improvement in spatial resolution between UHR and conventional NR imaging.[12] However, there has been no direct comparison between SHR and UHR imaging specifically. Our preliminary data suggest that there is no statistically significant difference in subjective image quality between UHR and SHR imaging, which differs mainly in the reconstruction matrix size of 1,024 versus 2,048, respectively. Radiation doses were identical for SHR and UHR imaging. The fact that the temporal bone is an intrinsically high signal-to-noise structure is likely an important contributing factor to this finding.

Higher resolution spatial imaging may overcome some of the shortcomings of current temporal bone imaging. More accurate ossicular prosthetic dimensions measured on higher spatial resolution CT can improve hearing and functional outcomes. For example, conventional CT

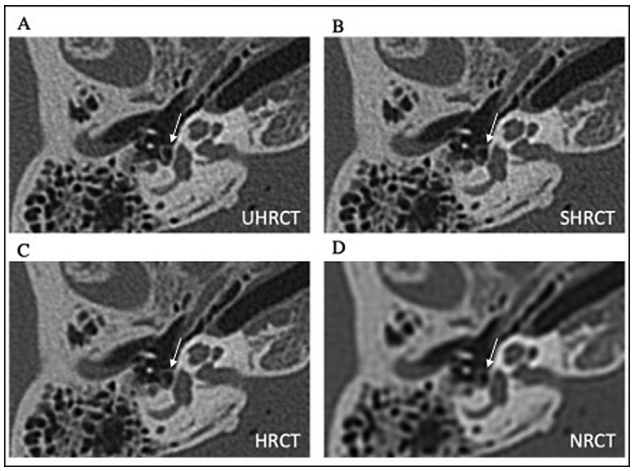

Fig. 1 Axial images of the stapes acquired at (**A**) ultra-high resolution, (**B**) super-high resolution, (**C**) high resolution, and (**D**) normal resolution. Super- and ultra-high-resolution CT imaging demonstrates improve visualization of the stapes crura. Air is seen within the petrous carotid canal and intracranially secondary to the use of cadaveric specimens.

measurements consistently overestimated intravestibular piston dimensions and vestibular intrusion for stapedial protheses.[25] Better pre- and postoperative assessments of cochlear implant patients can guide decisions regarding candidacy for surgery, side selection, surgical technique, and the detection of postoperative complications.[4] However, metallic artifacts from implants will still present a diagnostic challenge irrespective of spatial resolution. Different acquisition techniques and metal artifact reduction algorithms can be applied to reduce CT metal artifacts, which can be further investigated on this high-resolution CT system in the future. 3D printing of the anatomy of the temporal bone utilizing higher spatial resolution CT for better detailed delineation of small osseous structures can be helpful for educational and surgical teaching.[26]

Limitations of this study includes a small sample size and use of cadaveric specimens, which was necessary to eliminate radiation dose from being a limiting factor in this comparative analysis. We used the FC35 standard sharp bone reconstruction kernel. Although it is not a high-resolution kernel, it is the most commonly used kernel at our institution. Future investigations can be focused on the relative image quality of SHR and UHR imaging in patients.

Potential Clinical Impact

Our preliminary data indicate that the SHR dataset can still capture the highest anatomic detail of the temporal bone relative to the UHR dataset, while requiring lesser computational requirements and shorter reconstruction times, which is conducive for efficient workflow. Greater anatomic detail is clinically important for several reasons. This information can potentially improve the diagnosis, surgical treatments,[27,28] and accuracy of 3D-printed models[29–32] of temporal bone diseases.

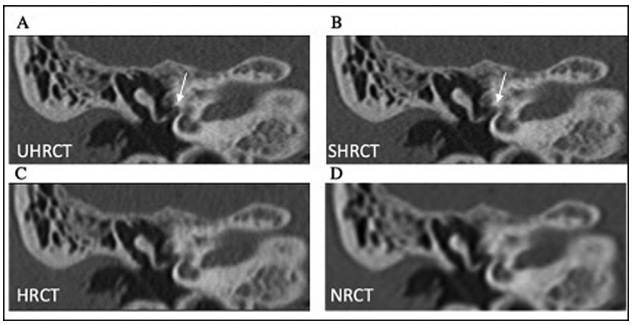

Fig. 2 Coronal images of the malleus, incus, and stapes acquired at (**A**) ultra-high resolution, (**B**) super-high resolution, (**C**) high resolution, and (**D**) normal resolution. The stapes crura are better demonstrated on super- and ultra-high-resolution CT imaging.

Conclusion

Super-high-resolution and ultra-high-resolution CT imaging results in significant improvement in image quality compared with normal-resolution and high-resolution CT imaging of the temporal bone. This study also indicates that there is no significant clinically relevant difference in image quality between super-high-resolution and ultra-high-resolution CT imaging of the temporal bone.

Conflict of Interest
None declared.

References

1 Jäger L, Bonell H, Liebl M, et al. CT of the normal temporal bone: comparison of multi- and single-detector row CT. Radiology 2005;235(01):133–141
2 Koesling S, Kunkel P, Schul T. Vascular anomalies, sutures and small canals of the temporal bone on axial CT. Eur J Radiol 2005; 54(03):335–343
3 Bartling SH, Gupta R, Torkos A, et al. Flat-panel volume computed tomography for cochlear implant electrode array examination in isolated temporal bone specimens. Otol Neurotol 2006;27(04): 491–498
4 Gleeson TG, Lacy PD, Bresnihan M, Gaffney R, Brennan P, Viani L. High resolution computed tomography and magnetic resonance imaging in the pre-operative assessment of cochlear implant patients. J Laryngol Otol 2003;117(09):692–695
5 Kahn JB, Stewart MG, Diaz-Marchan PJ. Acute temporal bone trauma: utility of high-resolution computed tomography. Am J Otol 2000;21(05):743–752
6 Stone JA, Castillo M, Neelon B, Mukherji SK. Evaluation of CSF leaks: high-resolution CT compared with contrast-enhanced CT and radionuclide cisternography. AJNR Am J Neuroradiol 1999;20 (04):706–712
7 Yamashita K, Yoshiura T, Hiwatashi A, et al. The radiological diagnosis of fenestral otosclerosis: the utility of histogram analysis using multidetector row CT. Eur Arch Otorhinolaryngol 2014; 271(12):3277–3282
8 Yamashita K, Yoshiura T, Hiwatashi A, et al. Contributing factors in the pathogenesis of acquired cholesteatoma: size analysis based on MDCT. AJR Am J Roentgenol 2011;196(05):1172–1175
9 Yiin RS, Tang PH, Tan TY. Review of congenital inner ear abnormalities on CT temporal bone. Br J Radiol 2011;84(1005):859–863
10 Yuen HY, Ahuja AT, Wong KT, Yue V, van Hasselt AC. Computed tomography of common congenital lesions of the temporal bone. Clin Radiol 2003;58(09):687–693

11 Fatterpekar GM, Doshi AH, Dugar M, Delman BN, Naidich TP, Som PM. Role of 3D CT in the evaluation of the temporal bone. Radiographics 2006;26(1, Suppl 1):S117–S132
12 Yamashita K, Hiwatashi A, Togao O, et al. Ultrahigh-resolution CT scan of the temporal bone. Eur Arch Otorhinolaryngol 2018;275 (11):2797–2803
13 Hiraumi H, Obara M, Yoshioka K, Ehara S, Sato H. Detectability of minute temporal bone structures with ultra-high resolution CT. Auris Nasus Larynx 2019;46(06):830–835
14 Flohr TG, Stierstorfer K, Süss C, Schmidt B, Primak AN, McCollough CH. Novel ultrahigh resolution data acquisition and image reconstruction for multi-detector row CT. Med Phys 2007;34(05): 1712–1723
15 McCollough CH, Leng S, Sunnegardh J, et al. Spatial resolution improvement and dose reduction potential for inner ear CT imaging using a z-axis deconvolution technique. Med Phys 2013;40(06):061904
16 Meyer M, Haubenreisser H, Raupach R, et al. Initial results of a new generation dual source CT system using only an in-plane comb filter for ultra-high resolution temporal bone imaging. Eur Radiol 2015;25(01):178–185
17 Zhou W, Lane JI, Carlson ML, et al. Comparison of a photon-counting-detector CT with an energy-integrating-detector CT for temporal bone imaging: a cadaveric study. AJNR Am J Neuroradiol 2018;39(09):1733–1738
18 Leng S, Diehn FE, Lane JI, et al. Temporal bone CT: improved image quality and potential for decreased radiation dose using an ultra-high-resolution scan mode with an iterative reconstruction algorithm. AJNR Am J Neuroradiol 2015;36(09):1599–1603
19 Gupta R, Grasruck M, Suess C, et al. Ultra-high resolution flat-panel volume CT: fundamental principles, design architecture, and system characterization. Eur Radiol 2006;16(06): 1191–1205
20 Kalender WA, Kyriakou Y. Flat-detector computed tomography (FD-CT). Eur Radiol 2007;17(11):2767–2779
21 Gupta R, Cheung AC, Bartling SH, et al. Flat-panel volume CT: fundamental principles, technology, and applications. Radiographics 2008;28(07):2009–2022
22 Ross W, Cody DD, Hazle JD. Design and performance characteristics of a digital flat-panel computed tomography system. Med Phys 2006;33(06):1888–1901
23 Oostveen LJ, Boedeker KL, Brink M, Prokop M, de Lange F, Sechopoulos I. Physical evaluation of an ultra-high-resolution CT scanner. Eur Radiol 2020;30(05):2552–2560
24 Yanagawa M, Hata A, Honda O, et al. Subjective and objective comparisons of image quality between ultra-high-resolution CT and conventional area detector CT in phantoms and cadaveric human lungs. Eur Radiol 2018;28(12):5060–5068
25 Hahn Y, Diaz R, Hartman J, Bobinski M, Brodie H. Assessing stapes piston position using computed tomography: a cadaveric study. Otol Neurotol 2009;30(02):223–230
26 Wiet GJ, Stredney D, Powell K, Hittle B, Kerwin T. Integration of high-resolution data for temporal bone surgical simulations. Int J CARS 2016;11(10):1845–1854
27 Arndt S, Kromeier J, Berlis A, Maier W, Laszig R, Aschendorff A. Imaging procedures after bone-anchored hearing aid implantation. Laryngoscope 2007;117(10):1815–1818
28 Connor SEJ. Contemporary imaging of auditory implants. Clin Radiol 2018;73(01):19–34
29 Rose AS, Webster CE, Harrysson OL, Formeister EJ, Rawal RB, Iseli CE. Pre-operative simulation of pediatric mastoid surgery with 3D-printed temporal bone models. Int J Pediatr Otorhinolaryngol 2015;79(05):740–744
30 Hirsch JD, Vincent RL, Eisenman DJ. Surgical reconstruction of the ossicular chain with custom 3D printed ossicular prosthesis. 3D Print Med 2017;3(01):7
31 Mitsouras D, Liacouras P, Imanzadeh A, et al. Medical 3D printing for the radiologist. Radiographics 2015;35(07):1965–1988
32 Ballard DH, Trace AP, Ali S, et al. Clinical applications of 3D printing: primer for radiologists. Acad Radiol 2018;25(01):52–65